Ocean Sci., 18, 1419–1430, 2022
https://doi.org/10.5194/os-18-1419-2022

Ocean Science Open Access EGU

Upper-ocean response to the passage of tropical cyclones in the Azores region

Miguel M. Lima[1], **Célia M. Gouveia**[1,2], **and Ricardo M. Trigo**[1,3]

[1]Instituto Dom Luiz (IDL), Faculdade de Ciências, Universidade de Lisboa, 1749-016, Lisbon, Portugal
[2]Instituto Português do Mar e da Atmosfera (IPMA), I.P., 1749-077, Rua C do Aeroporto, Lisbon, Portugal
[3]Departamento de Meteorologia, Universidade Federal do Rio de Janeiro, Rio de Janeiro 21941-919, Brasil

Correspondence: Miguel M. Lima (malima@fc.ul.pt)

Received: 8 March 2022 – Discussion started: 10 March 2022
Revised: 21 July 2022 – Accepted: 27 July 2022 – Published: 29 September 2022

Abstract. Tropical cyclones (TCs) are extreme climate events that are known to strongly interact with the ocean through two mechanisms: dynamically through the associated intense wind stress and thermodynamically through moist enthalpy exchanges at the ocean surface. These interactions contribute to relevant oceanic responses during and after the passage of a TC, namely the induction of a cold wake and the production of chlorophyll (Chl *a*) blooms. This study aimed to understand these interactions in the Azores region, an area with relatively low cyclonic activity for the North Atlantic basin, since the area experiences much less intense events than the rest of the basin. Results for the 1998–2020 period showed that the averaged induced anomalies were on the order of $+0.050\,\mathrm{mg\,m^{-3}}$ for Chl *a* and $-1.615\,^{\circ}\mathrm{C}$ for SST (sea surface temperature). Furthermore, looking at the role played by several TCs characteristics we found that the intensity of the TCs was the most important condition for the development of upper-ocean responses. Additionally, it was found that bigger TCs caused greater induced anomalies in both variables, while faster ones created greater Chl *a* responses, and TCs that occurred later in the season had greater TC-related anomalies. Two case studies (Ophelia in 2017 and Nadine in 2012) were conducted to better understand each upper-ocean response. Ophelia was shown to affect the SST at an earlier stage, while the biggest Chl *a* induced anomalies were registered at a later stage, allowing the conclusion that thermodynamic exchanges conditioned the SST more while dynamical mixing might have played a more important role in the later stage. Nadine showed the importance of the TC track geometry, revealing that the TC track observed in each event can impact a specific region for longer and therefore result in greater induced anomalies.

1 Introduction

Tropical cyclones (TCs) are potentially intense atmospheric disturbances which are characterised by a low-pressure centre (eye) which strong winds curl around. Among other important properties, TCs are thermodynamically dependent phenomena, meaning that intense temperature gradients need to occur in the lower atmosphere to maintain and intensify the storm. Thus, TCs are fed from warm seawater which provide a strong moist enthalpy flux from the oceanic surface to maintain a steep temperature gradient within the lower and middle troposphere and produce massive water vapour convection (Emanuel, 2003; Holton and Hakim, 2012; Pearce, 1987).

The strong wind stress present near the surface and the associated intense curl are also shown to induce vertical mixing and Ekman upwelling in the upper layer of the ocean. In his seminal study, Price (1981) shows, through both observed and numerical modelling data, the evolution of sea surface temperature (SST) in the passage of a hurricane, with the emergence of a cold wake of SST after a TC due to entrainment of water from deeper layers. This effect has since been well studied and documented with many case studies observed, for example, the case of Hurricane Felix, in the vicinity of Bermuda in 1995, which showed decreases in the order of 3.5–4 °C (Dickey et al., 1998), or the cases of cyclones Nargis (2008) and Laila (2010), in the Bay of Bengal, which caused SSTs to drop by around 1.76 °C (Maneesha et al., 2012). Additionally, several model-based works focused on either the effects caused by the TCs or the interaction of the TC with its own cold wake (e.g. Chen et al., 2017; Zhang et al., 2019).

There are also biological responses to the passage of a TC. Due to the upwelling of colder water, transport of nutrient-rich water from the sub-superficial layer may also occur (Kawai and Wada, 2011). In this case, phytoplankton can quickly increase in the surface layer following the rise in nutrients. This increase can be remotely sensed through satellite observations that capture the chlorophyll *a* concentration (Chl *a*) increasing after the passage of a TC, since Chl *a* is generally accepted as a proxy for biological activity (Kawai and Wada, 2011; Liu et al., 2009; Subrahmanyam et al., 2002; Walker et al., 2005).

The oceanic response, either physical or biological, to the passage of a TC depends on various aspects, most remarkably the TC's intensity and its translation speed but also the oceanic subsurface conditions (Zheng et al., 2008). The magnitude and significance of these aspects for the modulation of the oceanic response vary regionally, although it is generally seen that the most impactful phenomena are intense and slow TCs (Chacko, 2019; Price, 1981; Price et al., 1994). Recent studies (e.g. Chacko, 2019; Pan et al., 2018; Shropshire et al., 2016) have shown that regional differences do matter when studying the biological response. In the case of the Bay of Bengal, it was shown that the intensity of a TC is less important, and the most meaningful aspects are the TCs' translation speed and, to a lesser degree, a pre-existing shallow mixed layer (Chacko, 2019). The results from this study show that it is important to stress that relatively weaker TCs can also induce a strong biological response after their passage.

Until now, the Azores region has not been studied regarding its thermodynamic and biological impacts. This section of the North Atlantic (NA) basin presents much fewer and weaker cyclones than the tropical band of the basin, with this region being mainly a zone where TCs undergo either cyclosis or post-tropical transition into extra-tropical cyclones or midlatitude storms (Baatsen et al., 2015; Haarsma et al., 2013). The north-eastern Atlantic (NEA) Basin, where the Azores archipelago is located, presents significantly less TCs than the western counterpart, closer to the US coast (Baatsen et al., 2015; Lima et al., 2021; Haarsma et al., 2013). However, there is growing evidence of a significant increase in the frequency of strong TCs in both western (Kossin et al., 2020) and eastern (Lima et al., 2021) halves of the North Atlantic Ocean. The climatology of the area points to a south–north gradient in both SST and Chl *a*, with a decrease in the former and an increase in the latter (Amorim et al., 2017; Caldeira and Reis, 2017). In general, the southern part of the Azores region offers SSTs high enough to maintain TCs, although the necessary atmospheric conditions (e.g. high lapse rates and low wind shear) need to occur for their passage north-east through the Azores (Lima et al., 2021). However, this area is undergoing a transition due to anthropogenic climate change, and an increase both in number and intensity of TCs is expected (Baatsen et al., 2015; Haarsma et al., 2013). Therefore, the NEA Basin is a challenging study region to assess the impact that lower-intensity TCs have on the oceanic surface.

The main aim of this study is to analyse in detail the upper-ocean response observed after the passage of a TC in the Azores region, which is characterised by its lower-than-normal cyclonic activity in relation to the rest of the North Atlantic basin. In particular, we aim to evaluate the impacts on SST and Chl *a* concentration produced by important TC characteristics (averaged maximum wind speed, average translation speed, overall impacted area, time of occurrence, and geometry of the track). Two practical case studies, relative to Nadine (2012) and Ophelia (2017) are then thoroughly analysed to reflect the conclusions drawn for this area.

2 Data

The main data used to evaluate the oceanic response in this study are divided into three main parts: remotely sensed interpolated data used to characterise the Chl *a* and SST and TC track data, which provides the necessary additional information on the location and dynamic variables of each TC, which allow us to explore the oceanic response in the aforementioned data. Additionally, non-interpolated datasets are used for the case studies to validate the interpolated ones, and wind stress data are used for the Hurricane Ophelia case study.

Biological oceanic response was evaluated using a multisensor daily Chl *a* product available through the Copernicus Marine Environment Monitoring Service (CMEMS) in a $4\,\mathrm{km} \times 4\,\mathrm{km}$ resolution from the end of 1997 to the present (CMEMS, 2021b). This product, delivered by the ACRI-ST company, is based on the Copernicus-GlobColour project and obtained by merging different sensors: SeaWiFS, MODIS, MERIS, VIIRS-SNPP&JPSS1, and OLCI-S3A&S3B. The final Chl *a* product is a mix of several algorithms that consider different water conditions, such as oligotrophic, mesotrophic, coastal, clear, and complex waters (Garnesson et al., 2019). To produce a "cloud-free" product, the resulting data were subjected to daily interpolation to fill any gaps (Krasnopolsky et al., 2016; Saulquin et al., 2019). The lack of gaps in this dataset is particularly relevant in the context of this study since the areas analysed will be concentrated around the TCs; it is then expected that large amounts of the analysed areas would be under cloud coverage and, therefore, some of the analysed data are not real but interpolated values. Nonetheless, CMEMS provides approximate uncertainty levels for these data, which we used to assess the quality of our results. For further validation purposes we also used a non-interpolated Chl *a* product generated by the Ocean Colour component of the European Space Agency's Climate Change Initiative project (OC-CCI) (Sathyendranath et al., 2019). This dataset results from the merging of several sensors: SeaWiFS LAC and GAC, MODIS Aqua, MERIS, VIIRS, and OLCI. ESA's OC-CCI version 5.0 Chl *a* prod-

uct has a 0.042° resolution and a daily temporal resolution (Sathyendranath et al., 2021).

To evaluate the physical oceanic response and to relate this to the biological one, a daily SST dataset from the CMEMS was used, with a 0.05° resolution. These data are available from 1981 up to the near present (CMEMS, 2021a). Similarly to the previous CMEMS interpolated Chl *a* product, the SST field is also a blended gap-free analysis product, with the present one resulting from reprocessed (A)ATSR, SLSTR, and AVHRR sensor data being applied to the Operational SST and Sea Ice Analysis (OSTIA) system (Donlon et al., 2012). This reprocessed analysis product provides an estimate of the SST at 20 cm depth. The inputs to the system are SSTs at 10:30 and 22:30 local time, which means that the analyses roughly correspond to the daily average SST (Good et al., 2020; Lavergne et al., 2019; Merchant et al., 2013). As stated before, approximated error values for SST are also provided by CMEMS. Additionally, AVHRR Pathfinder version 5.3 collated data were used as non-interpolated data for validation. This dataset, similarly to the CMEMS one, is a collection of a twice daily (averaged to daily), 4 km spatial resolution, merged SST product, provided by NOAA's National Centers for Environmental Information (Saha et al., 2018). The merging of these data, however, is only used to spatially collate the data, as they are a single instrument measurement (AVHRR) onboard NOAA-7 through NOAA-19 Polar Operational Environmental Satellites (POES).

Wind stress data to assist in the analysis of the Hurricane Ophelia case study were provided by NOAA's CoastWatch dataset available at https://coastwatch.pfeg.noaa.gov/erddap/griddap/erdQMstress1day_LonPM180.html. This dataset is derived from wind measurements obtained from the Advanced Scatterometer (ASCAT) instrument on board EUMETSAT's MetOp satellites (A and B) at a daily 0.25° resolution, from 2013 to the present. ASCAT presents a near all-weather capacity (not affected by clouds), as it operates a frequency in C-band (5.255 GHz), therefore, minimising the number of missing values in predominately clouded areas such as the case of TC paths.

The TC track data are made available by the International Best Track Archive for Climate Stewardship Project version 4 (IBTrACS v4) free-access dataset (Knapp et al., 2010). This dataset contains global information regarding TC activity from the 1851 hurricane season up to 2020. It aggregates variables such as TC geographical location, maximum wind speed, minimum sea level pressure, and storm radius estimation based on wind intensity, measured at 6 h intervals (original dataset interpolates for increased resolution, at 3 h rates; however this interpolation only includes the geographical location). For the 1998–2020 period, the Azores region experienced the passage of 62 individual TCs accounting to 642 6 h observations that are categorised in the following intensities according to the Saffir–Simpson hurricane wind scale (Taylor et al., 2010):

- 148 tropical depression observations
- 389 tropical storm observations
- 85 category 1 hurricane observations
- 18 category 2 hurricane observations
- 2 category 3 hurricane observations.

The full TC tracks can be better visualised in Fig. 1, with panel (a) showing the full track for all these 62 TCs observed in the NA basin for the 1998–2020 period and panel (b) showing a zoomed view relative to the considered Azores region. Tropical depression observations (dark blue in Fig. 1b) account for 23 % of the total observations and will not be considered in this study, as they present the lower branch of intensities with winds below the 34 kt (18 m s^{-1}) threshold. Therefore, a total of 494 TC 6 h observations were considered for this study.

Since the interpolated datasets used for most of this study do not share the same timeframe and to better encapsulate full years of data, the timeframe of the present study will be from 1 January 1998 to 31 December 2020. Moreover, while we have extracted all the data described above covering the entire North Atlantic basin, we will focus on the area around the Azores archipelago, delimited by the 15° W and 40° W meridians and between the 30° N and the 45° N parallels (Fig. 1).

3 Methodology

The region of study was chosen due to its nature regarding TCs, since it is an area with fewer and less intense tropical storms (Hart and Evans, 2001; Lima et al., 2021; Ramsay, 2017). Generally, tropical cyclosis and post-tropical transition occur here (Baatsen et al., 2015; Haarsma et al., 2013). Because of these aspects, it corresponds to a much less studied area and is a good region to characterise oceanic biophysical effects after the passage of (generally) weaker TCs at higher-than-tropical latitudes and to compare the obtained results with previous literature.

To cope with large amounts of data, the biophysical response was evaluated within a small area around individual locations obtained for each TC's best-track location. For this, we used the approximated quadrant radius given by the IBTrACS v4 dataset. This dataset provides different types of radii depending on the considered isotach; for this study we used the 34 kt isotach as it corresponds to the lower bound for the tropical storm status according to the Saffir–Simpson hurricane wind scale (Taylor et al., 2010). Since the considered area of analysis falls above the 34 kt isotach, tropical depressions were not considered (exact partition of intensities is given at the end of Sect. 2). There are some missing radii values in the middle of the TC tracks, and, to correct those, a simple linear regression was applied. To illustrate the application of this methodology we present the case

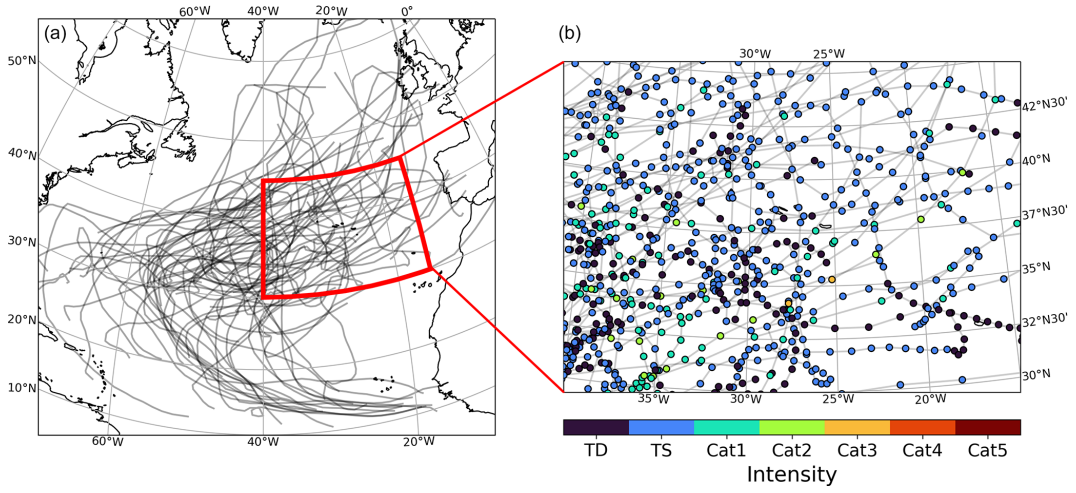

Figure 1. (a) North Atlantic basin and the tracks of all the TCs that went through or occurred inside the study region (shown by the red outline). **(b)** Zoom of the previous red outline, with each TC observation marked in different colours for intensity (TD: tropical depression; TS: tropical storm; Cat1–Cat5: hurricane category according to the hurricane Saffir–Simpson wind scale).

studies in Sect. 4, for hurricanes Ophelia (2017) and Nadine (2012). From inside this area of analysis, we may retrieve the Chl *a* concentration and SST at their respective resolution. The analysis inside the considered area was performed using histograms, in which each pixel inside the 34 kt isotach contributes to that TC's histogram.

To analyse the TCs' impact on their passage, inspiration was taken from Kawai and Wada (2011), who computed the climatic monthly standard deviation of Chl *a* on 0.25° grids over a 5-year study period. Here, we compute the daily normalised anomaly from the climatological value (in standard deviation units). For this, we first calculated the climatological mean and associated standard deviation of both Chl *a* and SST values for the region that is impacted by each TC on the day of analysis. This is achieved considering the 3 d before and 3 d after the day of analysis, totalling 1 week that is then retrieved from the entire study period of 22 years, thus ensuring a larger sample and a smoother continuous curve. Then, we compute the mean value in the same area (in which only the TC area was considered) for the day of analysis, and finally, we calculate the normalised anomaly from the climatology on that day. This analysis was performed considering 30 d before and after each TC to then allow the analysis and identification of an ideal window to compute the induced anomalies. To compute this ideal window, we searched for the maximum difference between the number of standard deviations over the climatological value before and after the storm.

To compromise between having the maximum difference and ensuring a time window as close as possible to the storm (to minimise external factors to the TC), we performed a sensibility study on the length and location of the considered time window. First, we analyse the overall maximum difference in the 61 d period (including the day of the storm) and then search for a secondary maximum value that is within 10 % of it, considering a smaller sample of days, decreasing in groups of 5 d each time this search is made (the first iteration would be 25 d before and 30 after, the second 30 before and 25 after, the third 25 before and after, etc.), until an optimum maximum difference value is identified. With this window defined, the induced (or TC-related) anomalies are simply the difference between the daily values of Chl *a* or SST after and before the TC.

As an example of this methodology, Fig. 2 shows the Chl *a* standard deviation over the climatological value in the case of Hurricane Nadine. In this case, only 15 d around the TC are shown for clarity. We can see that the maximum difference is obtained between 8 d before and 1 d after the storm (ΔChl *a* max). However, when we take into account the compromise of considering windows located as closely as possible to the occurrence of the TC over the region, we see that the value found between 4 d before and 1 d after is within 10 % of the absolute maximum. This methodology is then applied to all 6 h observations individually and for each TC, thus resulting in two groups of induced anomalies (per TC and per 6 h observations) where we can study these with respect to the TCs averaged (per TC) or instantaneous (6 h observations) characteristics.

To address the possibility that some pixels are overlaid on top of each other, which would contaminate the analysis, as observed in the case of the slow erratic Hurricane Nadine (presented in the "Results and discussion" section as a case study), we did not take into consideration the days in which the TC is over the aforementioned overlaid region. In the case of these pixels, the day considered to be after the TC is the day after it has completely passed over the area (i.e. the observations in that pixel during the days the TC is still over the area are discarded). However, when we consider inde-

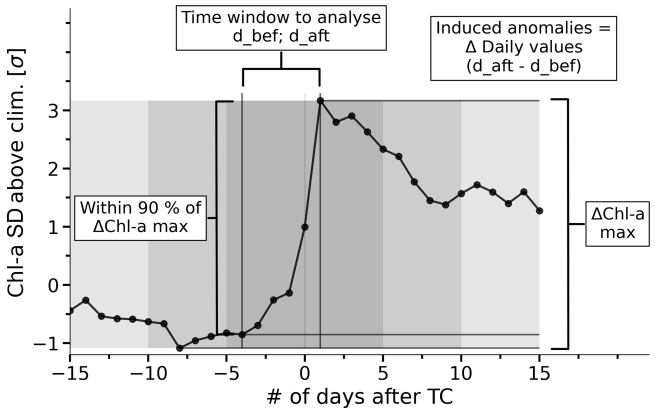

Figure 2. Schematic of the applied methodology for each TC. Black line shows the number of standard deviations from the climatological values for the area surrounding Hurricane Nadine. A detailed description of this methodology can be found in the text.

pendent 6 h observations, this caveat cannot be accounted for since we have no way of knowing if that area has been influenced or not by the TC before, for how long, or even if a future observation will impact the area.

As previously mentioned in Sect. 2, the interpolated data used for this study are expected to encounter some regions where clouds are to be expected due to the presence of the TCs. To account for this potential caveat, we looked at the uncertainties associated with the data before and after the TCs as well as during the TC (e.g. day 0 in Fig. 2), to evaluate if there were clear increases in uncertainty for cloud-covered situations.

Two case studies were looked at in greater detail: Hurricane Ophelia (2017) and Hurricane Nadine (2012). The former was performed to assess the different impacts along the life cycle of the storm, and different histograms were produced for smaller portions of the TC. The latter was made to analyse the possible increasing impacts the storm geometry could cause. Additionally, these case studies were used as validation for the interpolated cloud-free data, where a comparison was made between the non-interpolated and the interpolated cloud-free data described in Sect. 2.

4 Results and discussion

Applying the mentioned methodology leaves us with a large pool of induced anomalies, from which we can now evaluate the distribution of these TC-related anomalies for both Chl *a* and SST as shown in Fig. 3a and b in the form of histograms of induced Chl *a* and SST induced anomalies, respectively. Both variables present a large impact after the passage of TCs, with Chl *a* presenting a mean response of positive $0.050\,\mathrm{mg\,m^{-3}}$ and the SST showing a mean response of $-1.615\,^{\circ}\mathrm{C}$. Figure 3c–f show the corresponding distributions as a function of the cyclone's intensities (Fig. 3c and d) and translation speeds (Fig. 3e and f). To make these distinctions, we chose only the high values (either regarding intensity or translation speed) to be those above the third quartile and the lower values to be those below the second quartile.

Firstly, regarding intensity (Fig. 3c and d), we have the induced response of the most powerful intensities in orange and the weaker ones in blue. Regarding the impact as a function of intensity it is possible to observe that more powerful TCs tend to induce a stronger biological response than weaker ones, which have a mean response closer to zero. It is also important to note that the more powerful TCs have a response that is much more skewed towards extreme positive values of Chl *a*. Figure 3d also shows a great impact regarding different intensities in SST, in which even weaker TCs show a substantial mean response of $-1.517\,^{\circ}\mathrm{C}$ and nearly all the analysed pixels showing negative induced anomalies. It is important to note the nearly bimodal nature of this distribution, which can be attributed to both the earlier phase of TCs (more energy being drawn from the ocean) resulting in more negative SST values and the less negative corresponding to the later part of TCs since baroclinic instabilities are more prevalent than the action of moist enthalpy flux from the ocean at this phase (Baatsen et al., 2015; Emanuel, 2003). Powerful TCs induced a more varied distribution of induced anomalies, with a mean response of $-1.694\,^{\circ}\mathrm{C}$.

Regarding the different translation speeds, Fig. 3e shows that, for biological responses, faster TCs show a greater mean value of $+0.060\,\mathrm{mg\,m^{-3}}$. This difference is not as remarkable as the one in Fig. 3c. On the other hand, the SST response (Fig. 3f) seems to be weakly impacted by the TC's translation speed, with slower TCs having a slightly stronger impact than faster ones, while the mean response values do not differ as much as the ones in Fig. 3d. Additionally, even if faster TCs do not affect the SST response as much as slower ones, the mean value is still close to what is seen in the general case in Fig. 3b, and most of the impact is towards negative SSTs.

To quantify these relations, Fig. 4 shows the storm-averaged induced anomalies compared to the averaged maximum wind and average translation speed. The linear regression is also shown for each of the comparisons, with nearly all results significant at the 95 % statistical level. According to these plots, only the translation speed in relation to the SST induced anomalies (Fig. 4d) did not show a significant relation at the 95 % statistical confidence level (marked by the dashed regression line). Regarding the mean wind (Fig. 4a and c), and therefore the TC's average intensity within the Azores region, the linear regression showed significant values, upwards of 0.5 for Chl *a* and -0.3 for SST induced anomalies. In the case of Chl *a*, like observed in Fig. 3, the relation is positive while with SST this relation is negative. Considering the translation speed, the relation is equally positive and significant for biological responses ($r = 0.416$).

Further analysis of other TC characteristics requires a different approach. Figure 5 shows similar relations to Fig. 4 but

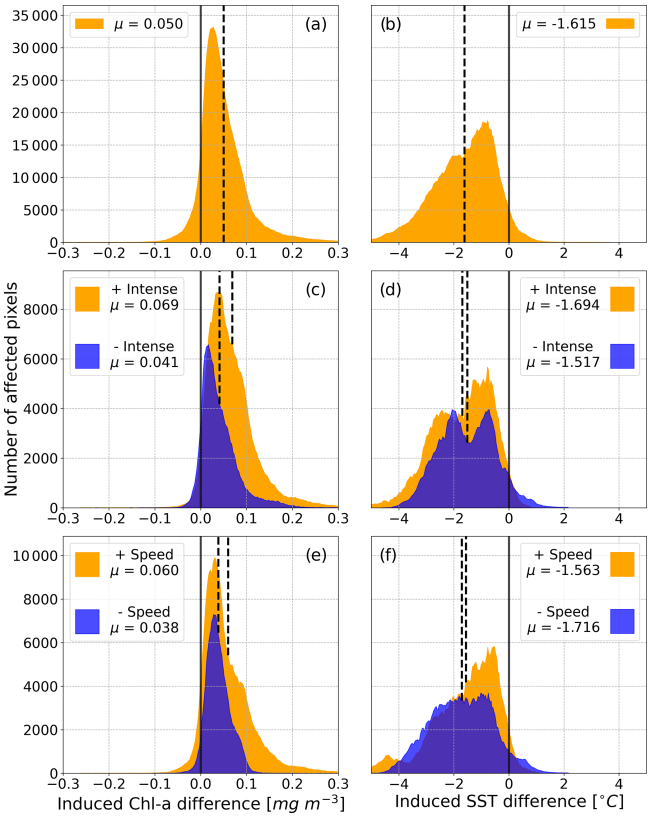

Figure 3. Histograms for **(a)** total Chl *a* and **(b)** SST induced anomalies; **(c)** Chl *a* and **(d)** SST induced anomalies after weak (blue) and powerful TCs (orange); **(e)** Chl *a* and **(f)** SST induced anomalies after slow TCs (blue) and fast TCs (orange). Each subplot histogram presents the respective population mean value (μ) as a dashed black line and the zero value as a grey line.

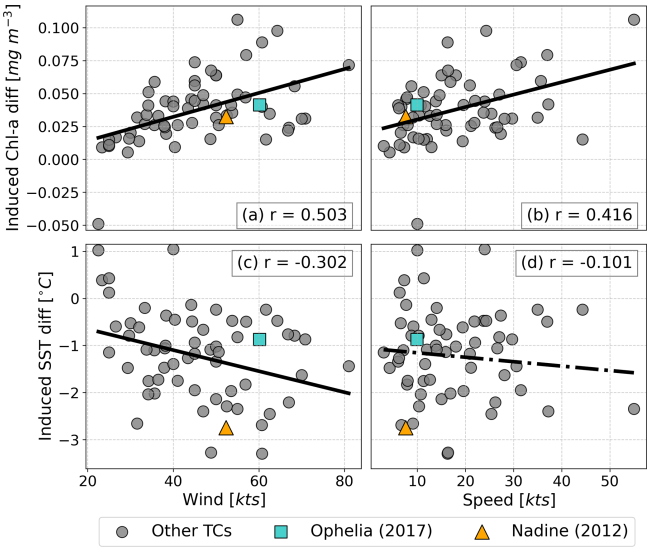

Figure 4. Linear regression of Chl *a* **(a, b)** and SST **(c, d)** induced anomalies for each TC, respectively, when compared with average winds in knots **(a, c)** and average TC translation speed in knots **(b, d)**. In each plot the Pearson *R* is presented, and the regression's significance is marked by the type of line used in the regression, with a dashed line representing non-significant regression at a 95 % confidence level and a solid line representing a regression significant at the 95 % confidence level.

considering 6 h observations instead of total TC mean values. This is made to account for the possible error that averaging a whole TC may create since the cyclone's characteristics may change substantially along its lifetime. This analysis, however, does not consider the possibility of superposition in pixels from observation to observation – i.e. from a TC that either moves slowly or whose track is more erratic, ending up covering the same area for several hours/days. This caveat was not present in Fig. 4 since we considered the TC lifetime as a whole and could then disregard the days of superposition. Using 6 h observations, we can study several types of characteristics that change between observations, such as the impact area or the time of season when it occurred, adding to the already seen maximum wind speed and translation speed.

Considering then the maximum wind speed per observation (Fig. 5a and e), both variables are significantly related to this characteristic, which is expected considering the analysis made in Figs. 3 and 4. As previously noted in the form of histograms in Fig. 3, most observations show a positive impact regarding Chl *a* and, especially for SST as most fall below zero, a negative change after a TC. The affected area (Fig. 5b and f) also presents a significant relation, although less intense than that observed with the maximum winds. However, it should be noted that this variable is linked to the mean winds, since more intense cyclones tend to be larger than less powerful ones, but also to the storm phase, since storms nearing their post-tropical transition tend to grow larger (Knaff et al., 2014). Translation speed is the less correlated variable of those studied (Fig. 5c and g), with only the biological response seeing a positive relation to this characteristic, agreeing with the previous results from Figs. 3 and 4. The time period in the season in which the TC occurs seems to also be important for the magnitude of the average induced anomaly seen in both variables (Fig. 5d and h) with late occurrences in the season showing greater responses respective to the signal of induced anomalies seen in Fig. 3a and b. Lastly, a geographical correlation was concluded not to be relevant for this study (not shown), as both variables were correlated with both latitude and longitude, and only non-significant relations were found.

The results presented so far in this study result from interpolated cloud-free data and should be quality assured to guarantee the integrity of the conclusions made previously. As mentioned in Sect. 2, CMEMS provides measures of uncertainty for the Chl *a* and SST datasets used. Thus, we have explored these values at different periods as a first step in validating the quality of the data. Figure S1 in the Supplement shows the associated uncertainty with respect to the absolute

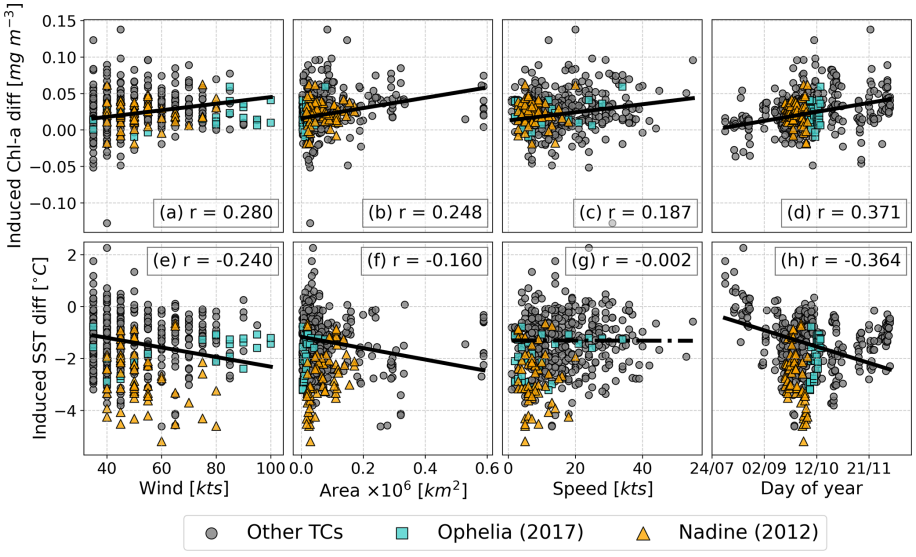

Figure 5. Same as in Fig. 4 but considering individual 6 h observations. Two columns are added: **(b)** and **(f)** with respect to the area affected by that observation and **(d)** and **(h)** with respect to the time of the year when that observation occurred.

observed values both for Chl *a* (top panels) and SST (bottom panels) for three different periods surrounding a TC event (before, during, and after) and a randomly drawn sample of the same size as the data analysed in the other subplots. It becomes immediately clear from these plots the considerably different magnitude of uncertainty for these data, with Chl *a* (Fig. S1a–d) ranging from 25 % to 45 % considering all moments, while SST (Fig. S1e–h) does not commonly surpass 0.4 % with a mean error around the 0.25 %. The randomly drawn sample of data gives a rough idea of the average uncertainty we can find in this dataset, with Chl *a* (Fig. S1a) presenting values around 35 % and SST (Fig. S1e) around 0.25 %. Additionally, we should consider three distinct moments of analysis, namely before and after the TC passage, which corresponds to the data used to compute the induced anomalies, and during the TCs, which should be the moment with most cloud cover over the studied regions. Looking first at Chl *a* (Fig. S1b–d) we see the progression from near-normal uncertainty before the TC (Fig. S1b) to an increase during TCs (Fig. S1c), likely due to the larger cloud-covered area in that situation. After the storm (Fig. S1d) however, the uncertainty substantially decreases reaching values below the randomly drawn sample (around 30 % compared to 35 %). For the SST (Fig. S1f–h), the associated uncertainty does not fluctuate substantially, constantly being below the 0.3 % mark. Additionally, the variation that has been identified before, with Chl *a* increasing and the SST decreasing, is noticeable in both variables.

Visible in Figs. 4 and 5 are two case studies: Hurricane Ophelia in 2017 (squares) and Hurricane Nadine in 2012 (triangles). These case studies were chosen based on the presented characteristics, coupled with the amount of sampling data within the region. Hurricane Ophelia (2017) was chosen due to its large intensity in the region (squares, Figs. 4 and 5), reaching a category 3 intensity on the Saffir–Simpson hurricane wind scale, something abnormal for the region (Lima et al., 2021). The complete TC track can be seen in the insert in Fig. 6a. Besides the large intensity, Ophelia's genesis took place inside our study region which enabled us to study different phases of the storm and its impacts on the ocean surface in the region. Even though Hurricane Ophelia was so intense, this storm impacted a very small area (Fig. 5b and f) particularly when compared with the other case study, Hurricane Nadine (2012). Hurricane Nadine (Fig. 7a) was chosen due to its large sampling, relatively high intensity (maximum category 1) and great impact area (second highest in this study, considering cumulative area of impact). The large impacted area was amplified by the geometry of the storm's track (i.e. many overlaid observations). Only the final stage of Hurricane Nadine was caught within the study region, producing an ideal case study to analyse the impact of a less intense storm that heavily impacted a particular region due to its geometry.

For the case study of Hurricane Ophelia (2017), three different phases of the storm were studied, corresponding approximately to cyclogenesis (Fig. 6a, triangles), maturing (Fig. 6a, squares), and mature hurricane (Fig. 6a, stars). There are 23 total observations; the first two phases encompass eight observations and the last one seven. Each of these phases has its own histogram in Fig. 6b and c (shown in colours), for the induced Chl *a* and SST TC-related anomalies, respectively. The histograms are inserted into a larger one (in black), representing the total induced anomalies caused by Ophelia, and therefore the sum of all three phases will result in the bigger histogram. Regarding the Chl *a* induced anomalies (Fig. 6b), Ophelia seemed to

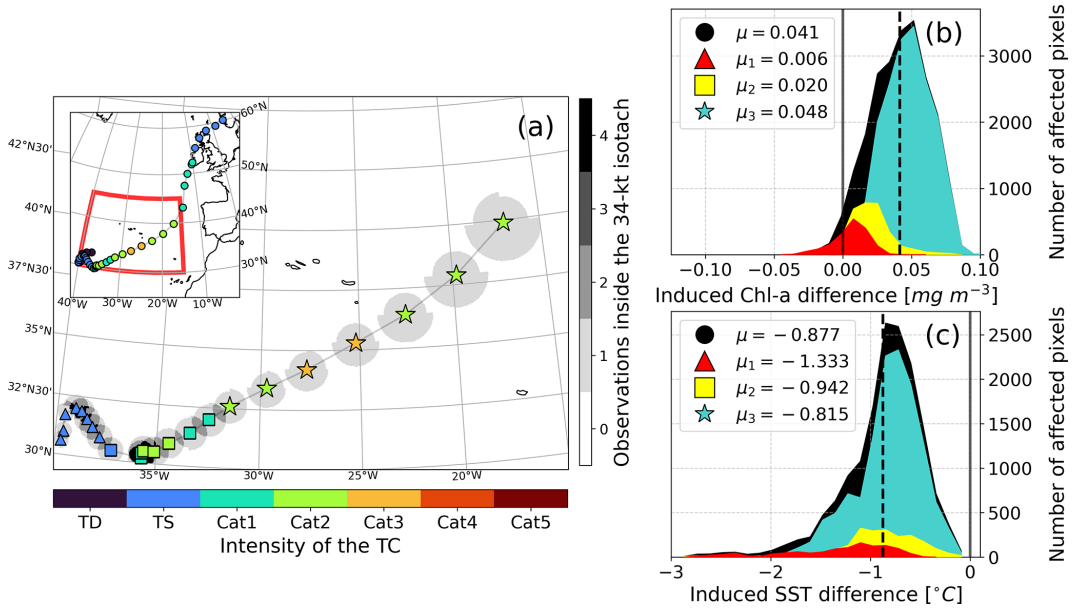

Figure 6. Case study for Hurricane Ophelia, in 2017, with its track on **(a)** (scatter marker colour scheme represents intensity as in Fig. 1), as well as the affected area around the cyclone (marked as the 34 kt isotach) with shading according to the number of pixels overlapping. There is an inset with the full track and the region of study marked with a red box. Ophelia's track is divided into three phases: histograms show induced Chl *a* **(b)** and SST induced anomalies **(c)** by phase of the storm (colours) and in total (black). The phase of the storm is marked in **(a)** as triangles (genesis), squares (maturing), and stars (mature) and correspond to the colours in **(b)** and **(c)**.

have a higher impact towards the end of its track in the region of study, when the storm had the highest intensity and the mean values of the induced anomalies increased along the track. Even at the storm's genesis, the induced anomalies were mostly positive with a mean value of $+0.006\,\mathrm{mg\,m^{-3}}$ reaching $+0.048\,\mathrm{mg\,m^{-3}}$ in the most intense phase. In contrast, the SST induced anomalies (Fig. 6c) present the highest mean response ($-1.333\,^{\circ}\mathrm{C}$) at the initial phase. The SST induced anomaly is then seen to decrease as the storm goes on, with the last phase weighing the most in the general distribution (as was seen for Chl *a*). The highest SST impact of the storm during the initial phases may reflect that this is the phase of the storm with highest interaction with the ocean, regarding thermodynamic exchanges (Emanuel, 2003).

As a further insight into Ophelia's interaction with the ocean surface, Fig. S2 shows the mean modulus of wind stress on the surface, by day of analysis (Fig. S2a) and by Ophelia's 6 h observations (Fig. S2b). Marked in both these plots are the analysed periods in corresponding colours and marker type to Fig. 6. These plots exceed the original study region, in order to fully encompass the TCs entire lifetime. There is a significant relation between the increased mean modulus of the wind stress and the evolution of the TC in time. This increase may be related to the increase in the storm's intensity. As Ophelia reaches its maximum intensity, so does the observed interaction with the ocean, decreasing afterwards as the storm moves north-eastward and undergoes post-tropical transition. This observed interaction with the ocean might be the reason for the maximum induced anomaly of Chl *a* being observed at the end of Ophelia's passage over the study region, inducing the mixing of the superficial layer.

Hurricane Nadine's (2012) case study shows very different behaviour and impact during its lifetime to that of Hurricane Ophelia. In this case, we present scatter plots of the averaged induced anomalies for the areas (Fig. 7b and c) corresponding to the superposition of pixels, i.e. the number of repeated observations inside the 34 kt isotach due to storm track geometry (as seen in Fig. 7a). The conclusions drawn regarding the Chl *a* and SST induced anomalies are similar and significant in this case study: the more time the TC spent over a certain area the more this area became affected by its passage, with large TC-related anomalies registered in both variables compared to less superposed ones (over $0.040\,\mathrm{mg\,m^{-3}}$ and $-3.500\,^{\circ}\mathrm{C}$ for Chl *a* and SST, respectively at 12 superposed pixels) and all cases being positive (negative) for Chl *a* (SST). It is possible to hypothesise that the translation speed also had a relevant role in these results, with a slower TC (Nadine was one of the slowest TCs in this study, as seen by the closer observations in Fig. 7a and by Figs. 4 and 5) spending more time over a region and therefore producing larger induced anomalies.

For these two case studies, we considered an additional quality assessment exercise, by comparing the interpolated cloud-free data to similar non-interpolated datasets. Figure 8 shows the histograms obtained for Ophelia and Nadine for

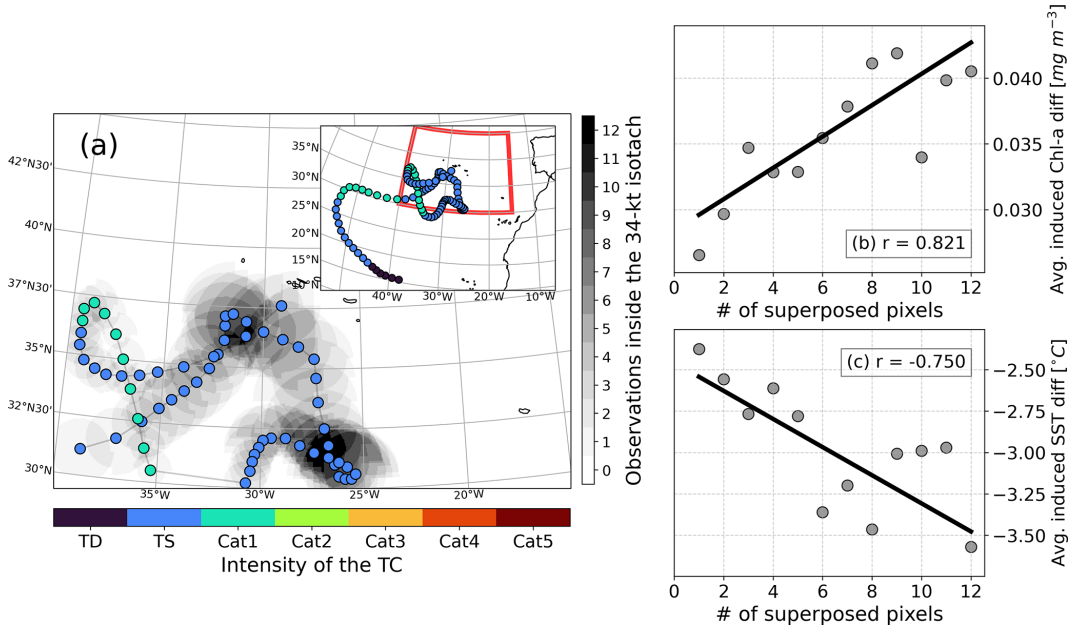

Figure 7. Case study for Hurricane Nadine, in 2012, with **(a)** the left panel the same as in Fig. 6. For Nadine, **(b)** and **(c)** pertain to the average induced Chl *a* and SST induced anomalies, respectively, based on the amount of superposition verified in each pixel.

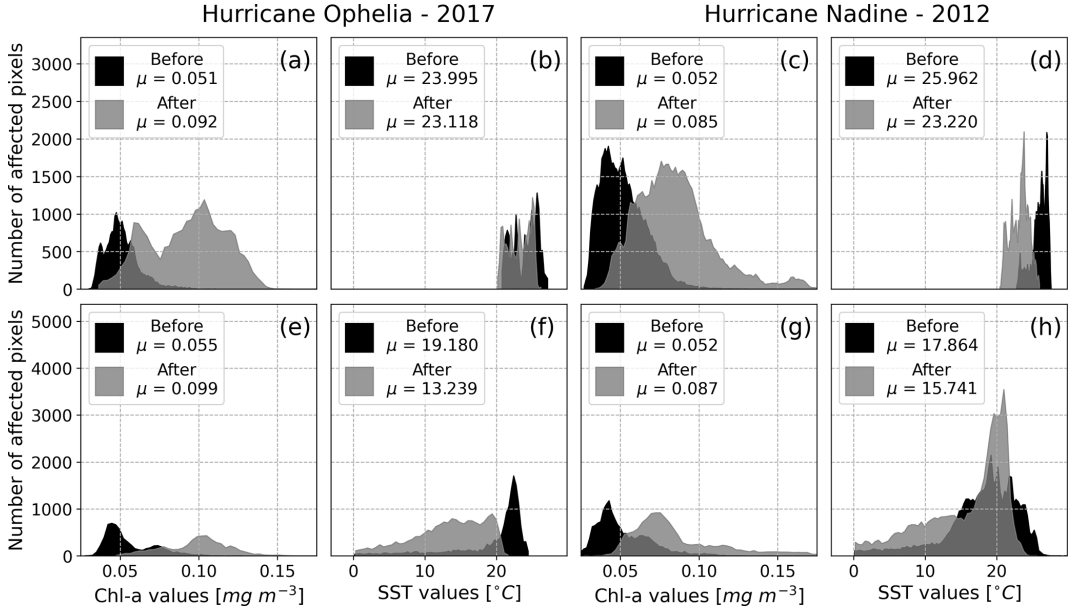

Figure 8. Comparison between interpolated "cloud-free" data **(a–d)** and non-interpolated data **(e–h)** for Hurricanes Ophelia (2017) and Nadine (2012). Values for non-interpolated data were obtained with the same methodology as the ones presented before and represent the exact same days of analysis. Mean values for each histogram are presented, with black histograms representing the situation before the TC and the grey ones the situation after.

the situations before and after the TC, independently, since non-interpolated data cannot be correctly subtracted as corresponding pixels may not be available. Overall, and despite the different number of observations considered, Chl *a* presents the same average response between the different types of data for both TCs, with non-interpolated data having an observed mean increase of 0.044 mg m^{-3} for Ophelia (Fig. 8e) compared to 0.041 mg m^{-3} for interpolated data (Fig. 8a), with these values representing the difference in the mean values shown in Fig. 8. Likewise, non-interpolated data reveal an increase of 0.035 mg m^{-3} for Nadine (Fig. 8g) compared to 0.033 mg m^{-3} for interpolated data (Fig. 8c).

Looking at the histograms, the shape of the data itself does not differ much between the different types, with peaks more or less located over the same values and distributions ranging over the same values. However, for the SST variable, despite both TCs presenting relatively similar decreases between both types of data, the non-interpolated data have a wider range of values, and the peaks do not correspond so closely. This, however, may be due to the process of data collation. In this process, some pixels are averaged with incorrect ones, resulting in unrealistic values in some areas. This can be identified by the unrealistic SST seen in Fig. 8f and h, with values that do not support TC development around 18–19 °C and reaching 0 °C. Nonetheless, interpolated SST data do show very low uncertainty as verified before (Fig. S1).

5 Final remarks

The current study provides the first general assessment of the biophysical oceanic response to the passage of TCs in a relatively low cyclonic activity area such as the region near the Azores archipelago. It is important to stress the efficiency of identifying the precise timing and associated spatial impacts of all TCs using remotely sensed products that rely on interpolated areas to fill existing gaps due to cloud coverage or lack of satellite imagery.

Over the Azores region, the existence of a biophysical response after the passage of a TC was identified from the analysis of Chl *a* and SST datasets, which produced signatures of positive Chl *a* and negative SST induced anomalies. This signature is more intense for the SST analysis, in which the passage of a TC results in nearly all observed pixels having a negative (i.e. cooling) induced anomaly. On average, TCs produced positive induced anomalies in the order of $0.050\,\mathrm{mg\,m^{-3}}$ regarding Chl *a* and a mean SST cooling of 1.615 °C.

The more powerful TCs tend to produce more intense biophysical oceanic responses, which agree with previous literature on the topic (Chacko, 2019; Price, 1981; Price et al., 1994). TC translation speed was also found to be associated with the induced anomalies, although the relationship was found to be positive and significant in the case of Chl *a* while it was not significant at the 95 % statistical confidence level for SST. The impacted area was also found to be significantly linked to the oceanic response. However, the sensitivity to the impacted area can rise due to several other factors: slower TCs impact larger areas (due to track geometry); more intense TCs impact larger areas (Knaff et al., 2014); and TCs nearing post-tropical transition are generally larger (Knaff et al., 2014). These effects, either individually or combined, can affect the induced anomalies at different levels. Additionally, the oceanic response was found to be larger later in the season, with significant relation in both variables. This may be due to the seasonal variability itself, as the normal climatological values for that time of the year are not seen during exceptional TC conditions (e.g. SST is usually colder but TC-prone conditions require it to be higher) (Amorim et al., 2017; Lima et al., 2021) and the oceanic response may help the impacted area return to values closer to the climatology, in both variables, in respect to that time of the year.

Two particular case studies were evaluated in further detail concerning hurricanes Ophelia (2017) and Nadine (2012). Hurricane Ophelia was a particular case as it corresponds to the only major hurricane in this study region and had almost its entire track inside this area. Ophelia showed strong induced anomalies for both Chl *a* and SST variables. Regarding Chl *a*, Ophelia had a stronger impact towards the end of its track within the region, revealing that its intensity played a key role in inducing Chl *a* TC-related anomalies, with the mean modulus of wind stress revealing a positive and significative relation to the evolution of the storm and therefore its intensity. On the other hand, Ophelia had a stronger impact on the SST in its cyclogenesis, probably related to ocean–atmosphere thermodynamic exchanges during its maturing. Hurricane Nadine, one of the slowest TCs in this study, showed more prominent induced anomalies, especially regarding SST. In this case, considering the low translational speed of Nadine, the objective was to study the impact that consecutive overlaid observations had on the induced anomalies. It is evident through this analysis that the impact increases with the number of superposed observations, implying that Nadine's slow translation speed and particular track geometry played a key role in creating such TC-related anomalies.

This study allowed for the quality control of both the remotely sensed cloud-free Chl *a* and SST multi-sensor products by comparing them to similar non-interpolated products and in the sense that it identified expected changes in the variables in areas covered by TC clouds and established crucial relations with some principal TC aspects. Future studies should aim to understand the inherent physical mechanisms that affect the ocean during and after the passage of a TC to better comprehend the associated induced anomalies.

Code and data availability. All code and raw data used to support the conclusion of this article will be made available by the authors upon request.

Supplement. The supplement related to this article is available online at: https://doi.org/10.5194/os-18-1419-2022-supplement.

Author contributions. MML was responsible for conceptualisation, methodology, software, validation, formal analysis, investigation, writing the original draft, review, and editing. CMG carried out validation, supervision, and writing (review and editing). RMT was responsible for validation, supervision, writing (review and editing), and funding acquisition.

Competing interests. The contact author has declared that none of the authors has any competing interests.

Disclaimer. Publisher's note: Copernicus Publications remains neutral with regard to jurisdictional claims in published maps and institutional affiliations.

Acknowledgements. Miguel M. Lima was supported by a grant through the project "DiscoverAZORES" PTDC/CTA-AMB/28511/2017 supported by the Portuguese Fundação para a Ciência e Tecnologia (FCT) I.P./MCTES. The authors also wish to thank the project "DiscoverAZORES", PTDC/C-TAAMB/28511/2017 for all the help/collaboration. The authors thank the anonymous reviewers for their thoughtful comments, suggestions, and efforts towards improving this work.

Financial support. This work was funded by the Portuguese Fundação para a Ciência e a Tecnologia (FCT) I.P./MCTES through national funds (PIDDAC) – UIDB/50019/2020.

Review statement. This paper was edited by Anne Marie Tréguier and reviewed by three anonymous referees.

References

Amorim, P., Perán, A. D., Pham, C. K., Juliano, M., Cardigos, F., Tempera, F., and Morato, T.: Overview of the ocean climatology and its variability in the Azores region of the North Atlantic including environmental characteristics at the seabed, Frontiers in Marine Science, 4, 56, https://doi.org/10.3389/fmars.2017.00056, 2017.

Baatsen, M., Haarsma, R. J., Van Delden, A. J., and de Vries, H.: Severe Autumn Storms in Future Western Europe with a Warmer Atlantic Ocean, Clim. Dynam., 45, 949–964, https://doi.org/10.1007/s00382-014-2329-8, 2015.

Caldeira, R. and Reis, J. C.: The Azores confluence zone, Frontiers in Marine Science, 4, 37, https://doi.org/10.3389/fmars.2017.00037, 2017.

Chen, S., Elsberry, R. L., and Harr, P. A.: Modelling interaction of a tropical cyclone with its cold wake, J. Atmos. Sci., 74, 3981–4001, https://doi.org/10.1175/JAS-D-16-0246.1, 2017.

Chacko, N.: Differential chlorophyll blooms induced by tropical cyclones and their relation to cyclone characteristics and ocean preconditions in the Indian Ocean, J. Earth Syst. Sci., 128, 1–11, https://doi.org/10.1007/s12040-019-1207-5, 2019.

CMEMS: ESA SST CCI and C3S reprocessed sea surface temperature analyses, CMEMS [data set], https://resources.marine.copernicus.eu/productdetail/SST_GLO_SST_L4_REP_OBSERVATIONS_010_011/INFORMATION (last access: 20 May 2022), 2021a.

CMEMS: Global ocean chlorophyll, PP and PFT (copernicus-globcolour) from satellite observations: Monthly and daily interpolated (reprocessed from 1997), CMEMS [data set], https://resources.marine.copernicus.eu/productdetail/OCEANCOLOUR_GLO_BGC_L4_MY_009_104/INFORMATION (last access: 6 April 2022), 2021b.

Dickey, T., Frye, D., McNeil, J., Manov, D., Nelson, N., Sigurdson, D., Jannasch, H., Siegel, D., Michaels, T., and Johnson, R.: Upper-ocean temperature response to Hurricane Felix as measured by the Bermuda Testbed Mooring, Mon. Weather Rev., 126, 1195–1201, https://doi.org/10.1175/1520-0493(1998)126<1195:UOTRTH>2.0.CO;2, 1998.

Donlon, C. J., Martin, M., Stark, J., Roberts-Jones, J., Fiedler, E., and Wimmer, W.: The operational sea surface temperature and sea ice analysis (OSTIA) system, Proc. SPIE, 116, 140–158, https://doi.org/10.1016/j.rse.2010.10.017, 2012.

Emanuel, K.: Tropical Cyclones, Annu. Rev. Earth Pl. Sc., 31, 75–104, https://doi.org/10.1146/annurev.earth.31.100901.141259, 2003.

Garnesson, P., Mangin, A., Fanton d'Andon, O., Demaria, J., and Bretagnon, M.: The CMEMS GlobColour chlorophyll a product based on satellite observation: multi-sensor merging and flagging strategies, Ocean Sci., 15, 819–830, https://doi.org/10.5194/os-15-819-2019, 2019.

Good, S., Fiedler, E., Mao, C., Martin, M. J., Maycock, A., Reid, R., Roberts-Jones, J., Searle, T., Waters, J., While, J., and Worsfold, M.: The current configuration of the OSTIA system for operational production of foundation sea surface temperature and ice concentration analyses, Remote Sens.-Basel., 12, 720, https://doi.org/10.3390/rs12040720, 2020.

Haarsma, R. J., Hazeleger, W., Severijns, C., de Vries, H., Sterl, A., Bintanja, R., Van Oldenborgh, G. J., and Van den Brink, H. W.: More Hurricanes to Hit Western Europe Due to Global Warming, Geophys. Res. Lett., 40, 1783–1788, https://doi.org/10.1002/grl.50360, 2013.

Hart, R. E. and Evans, J. L.: A climatology of the extratropical transition of Atlantic tropical cyclones, J. Climate, 14, 546–564, https://doi.org/10.1175/1520-0442(2001)014<0546:ACOTET>2.0.CO;2, 2001.

Holton, J. R. and Hakim, G. J.: An Introduction to Dynamic Meteorology, 5th Edn., Vol. 88, Academic Press, Elsevier, San Diego, CA, https://doi.org/10.1119/1.1987371, 2012.

Kawai, Y. and Wada, A.: Detection of cyclone-induced rapid increases in chlorophyll-*a* with sea surface cooling in the northwestern Pacific Ocean from a MODIS/SeaWiFS merged satellite chlorophyll product, Int. J. Remote Sens., 32, 9455–9471, https://doi.org/10.1080/01431161.2011.562252, 2011.

Knaff, J. A., Longmore, S. P., and Molenar, D. A.: An objective satellite-based tropical cyclone size climatology, J. Climate, 27, 455–476, https://doi.org/10.1175/JCLI-D-13-00096.1, 2014.

Knapp, K. R., Kruk, M. C., Levinson, D. H., Diamond, H. J., and Neumann, C. J.: The International Best Track Archive for Climate Stewardship (IBTrACS), B. Am. Meteorol. Soc., 91, 363–376, https://doi.org/10.1175/2009BAMS2755.1, 2010.

Kossin, J. P., Knapp, K. R., Olander, T. L., and Velden, C. S.: Global Increase in Major Tropical Cyclone Exceedance Probability over the Past Four Decades, P. Natl. A. Sci. USA, 117, 11975–11980, https://doi.org/10.1073/pnas.1920849117, 2020.

Krasnopolsky, V., Nadiga, S., Mehra, A., Bayler, E., and Behringer, D.: Neural networks technique for filling gaps in satellite measurements: Application to ocean

color observations, Comput. Intel. Neurosc., 29, 6156513, https://doi.org/10.1155/2016/6156513, 2016.

Lavergne, T., Sørensen, A. M., Kern, S., Tonboe, R., Notz, D., Aaboe, S., Bell, L., Dybkjær, G., Eastwood, S., Gabarro, C., Heygster, G., Killie, M. A., Brandt Kreiner, M., Lavelle, J., Saldo, R., Sandven, S., and Pedersen, L. T.: Version 2 of the EUMETSAT OSI SAF and ESA CCI sea-ice concentration climate data records, The Cryosphere, 13, 49–78, https://doi.org/10.5194/tc-13-49-2019, 2019.

Lima, M. M., Hurduc, A., Ramos, A. M., and Trigo, R. M.: The Increasing Frequency of Tropical Cyclones in the Northeastern Atlantic Sector, Front. Earth Sci., 9, 745115, https://doi.org/10.3389/feart.2021.745115, 2021.

Liu, X., Wang, M., and Shi, W.: A study of a Hurricane Katrina–induced phytoplankton bloom using satellite observations and model simulations, J. Geophys. Res.-Oceans, 114, C03023, https://doi.org/10.1029/2008JC004934, 2009.

Maneesha, K., Murty, V. S. N., Ravichandran, M., Lee, T., Yu, W., and McPhaden, M. J.: Upper ocean variability in the Bay of Bengal during the tropical cyclones Nargis and Laila, Prog. Oceanogr., 106, 49–61, https://doi.org/10.1016/j.pocean.2012.06.006, 2012.

Merchant, C. J., Le Borgne, P., Roquet, H., and Legendre, G.: Extended optimal estimation techniques for sea surface temperature from the Spinning Enhanced Visible and Infra-Red Imager (SEVIRI), Proc. SPIE, 131, 287–297, https://doi.org/10.1016/j.rse.2012.12.019, 2013.

Pan, J., Huang, L., Devlin, A. T., and Lin, H.: Quantification of typhoon-induced phytoplankton blooms using satellite multi-sensor data, Remote Sens.-Basel, 10, 318, https://doi.org/10.3390/rs10020318, 2018.

Pearce, R. P.: The physics of hurricanes, Phys. Technol., 18, 215–223, 1987.

Price, J. F.: Upper ocean response to a hurricane, J. Phys. Oceanogr., 11, 153–175, https://doi.org/10.1175/1520-0485(1981)011<0153:UORTAH>2.0.CO;2, 1981.

Price, J. F., Sanford, T. B., and Forristall, G. Z.: Forced stage response to a moving hurricane, J. Phys. Oceanogr., 24, 233–260, https://doi.org/10.1175/1520-0485(1994)024<0233:FSRTAM>2.0.CO;2, 1994.

Ramsay, H.: The Global Climatology of Tropical Cyclones, Oxford Research Encyclopedia of Natural Hazard Science, Victoria, Australia, Oxford University Press, https://doi.org/10.1093/acrefore/9780199389407.013.79, 2017.

Saha, K., Zhao, X., Zhang, H., Casey, K. S., Zhang, D., Baker-Yeboah, S., Kilpatrick, K. A., Evans, R. H., Ryan, T., and Relph, J. M.: AVHRR Pathfinder version 5.3 level 3 collated (L3C) global 4 km sea surface temperature for 1981–Present, NOAA National Centers for Environmental Information [data set], https://doi.org/10.7289/v52j68xx, 2018.

Sathyendranath, S., Brewin, R. J. W., Brockmann, C., Brotas, V., Calton, B., Chuprin, A., Cipollini, P., Couto, A. B., Dingle, J., Doerffer, R., Donlon, C., Dowell, M., Farman, A., Grant, M., Groom, S., Horseman, A., Jackson, T., Krasemann, H., Lavender, S., Martinez-Vicente, V., Mazeran, C., Mélin, F., Moore, T. S., Müller, D., Regner, P., Roy, S., Steele, C. J., Steinmetz, F., Swinton, J., Taberner, M., Thompson, A., Valente, A., Zühlke, M., Brando, V. E., Feng, H., Feldman, G., Franz, B. A., Frouin, R., Gould, R. W., Hooker, S. B., Kahru, M., Kratzer, S., Mitchell, B. G., Muller-Karger, F. E., Sosik, H. M., Voss, K. J., Werdell, J., and Platt, T.: An ocean-colour time series for use in climate studies: the experience of the Ocean-Colour Climate Change Initiative (OC-CCI), Sensors, 19, 4285, https://doi.org/10.3390/s19194285, 2019.

Sathyendranath, S., Jackson, T., Brockmann, C., Brotas, V.; Calton, B., Chuprin, A., Clements, O., Cipollini, P., Danne, O., Dingle, J., Donlon, C., Grant, M., Groom, S., Krasemann, H., Lavender, S., Mazeran, C., Mélin, F., Müller, D., Steinmetz, F., Valente, A., Zühlke, M., Feldman, G., Franz, B., Frouin, R., Werdell, J., and Platt, T.: ESA Ocean Colour Climate Change Initiative (Ocean_Colour_cci): Version 5.0 Data, NERC EDS Centre for Environmental Data Analysis [data set], https://doi.org/10.5285/1dbe7a109c0244aaad713e078fd3059a, 2021.

Saulquin, B., Gohin, F., and Fanton d'Andon, O.: Interpolated fields of satellite-derived multi-algorithm chlorophyll-*a* estimates at global and European scales in the frame of the European Copernicus-Marine Environment Monitoring Service, J. Oper. Oceanogr., 12, 47–57, https://doi.org/10.1080/1755876X.2018.1552358, 2019.

Shropshire, T., Li, Y., and He, R.: Storm impact on sea surface temperature and chlorophyll a in the Gulf of Mexico and Sargasso Sea based on daily cloud-free satellite data reconstructions, Geophys. Res. Lett., 43, 12–199, https://doi.org/10.1002/2016GL071178, 2016.

Subrahmanyam, B., Rao, K. H., Srinivasa Rao, N., Murty, V. S. N., and Sharp, R. J.: Influence of a tropical cyclone on chlorophyll-*a* concentration in the Arabian Sea, Geophys. Res. Lett., 29, 22-1–22-4, https://doi.org/10.1029/2002GL015892, 2002.

Taylor, H. T., Ward, B., Willis, M., and Zaleski, W.: The saffir-simpson hurricane wind scale, Atmospheric Administration, Washington, DC, USA, 2010.

Walker, N. D., Leben, R. R., and Balasubramanian, S.: Hurricane-forced upwelling and chlorophyll-*a* enhancement within cold-core cyclones in the Gulf of Mexico, Geophys. Res. Lett., 32, L18610, https://doi.org/10.1029/2005GL023716, 2005.

Zhang, J., Lin, Y., Chavas, D. R., and Mei, W.: Tropical cyclone cold wake size and its applications to power dissipation and ocean heat uptake estimates. Geophys. Res. Lett., 46, 10177–10185, https://doi.org/10.1029/2019GL083783, 2019.

Zheng, Z. W., Ho, C. R., and Kuo, N. J.: Importance of pre-existing oceanic conditions to upper ocean response induced by Super Typhoon Hai-Tang. Geophys. Res. Lett., 35, L20603, https://doi.org/10.1029/2008GL035524, 2008.